Connections between response modes in a horizontally driven granular material

M. Medved
James Franck Institute and Department of Physics, University of Chicago, 5640 South Ellis Avenue, Chicago, Illinois 60637
(Received 30 October 2000; revised manuscript received 6 August 2001; published 22 January 2002)

The behavior of a horizontally vibrated quasi-two-dimensional granular system is observed over a wide range of time scales by mapping the velocity fields at the boundary by using high-speed video and decomposing the behavior of the system into the harmonic, subharmonic, and convective responses. The observed relationships between these responses, as well as the fast shearing and the gap that opens between the material and the sidewalls, lead to a refinement of the current convection model, and also reveal that shearing is completely accounted for by the harmonic response. We find that internal degrees of freedom are always significant under horizontal vibration, as the specific boundary conditions (open surface and horizontal driving) give rise to a surface layer whose motion is decoupled by a narrow shear band from that of the bulk. All observed responses are related to this shear band. For example, the specific shape of the shear band gives rise to the surprising presence of period doubling and period quadrupling. As compared to the case of vertical excitation, all the observed responses now arise through new mechanisms.

DOI: 10.1103/PhysRevE.65.021305 PACS number(s): 45.70.−n, 47.50.+d

I. INTRODUCTION

Under external excitation, a granular material can mimic the behavior of solids, liquids or gases, never behaving exactly like any of these phases of matter [1–15]. In addition, their jamming property links them to other disordered systems, e.g., glasses, spin glasses, or traffic [1,16–19]. This rich dynamics arises from a remarkably simple physics. Yet, its theoretical description is still incomplete, due to several factors. The macroscopic nature of the interactions between grains (collisions, rubbing) necessarily leads to dissipation, as the kinetic energy is transferred to the many degrees of freedom internal to the individual particles. Another complicating property of granular materials is less obvious: it has been found that in granular systems there is no clear separation of the relevant microscopic and macroscopic length scales [1,20]. The macroscopic variables, e.g., density or mean velocity, can change significantly over distances of only several particle diameters, rendering the statistical ''microscopic ensemble'' meaningless in these systems. In addition, the role of boundary conditions in experiment, and their application to theoretical calculations are poorly understood. All these problems notwithstanding, there has been a lot of effort put into formulating the theory of granular hydrodynamics, i.e., into describing the granular flow through a system of uniform and local partial differential equations [21–23]. This is a very challenging task, as even the possibility of achieving this appealing goal is yet uncertain, given recent evidence that granular materials are intrinsically nonlocal and history dependent [24].

Studying a horizontally vibrated system provides an opportunity to shed light on some of these issues, most notably, on the role of boundary conditions. Horizontal vibrations produce shear stresses at the free surface, and compression at the vertical side boundaries. This contrasts with the extensively studied case of vertical vibrations, where there is compression at the free surface, and shearing at the vertical walls. How do these differences affect the behavior of the system? In deep vertically vibrated systems, frictional shearing at the vertical boundaries drives the convection [4,25,26]. Under horizontal vibrations, convection is also driven by (gravity-induced) shear stresses that cause avalanching down the side walls [27,28]. Further, under both kinds of excitation, the fluidization is initiated at the top free boundary, even though the type of stress differs [28–30]. When is the response determined by the type of stress (shear versus compression) and when by the type of boundary (open versus closed)?

In addition to altering the boundary conditions, horizontal shaking introduces another change from vertical excitation: it restores the symmetry of excitation, $x \rightarrow -x$; $t \rightarrow t - T/2$. The symmetry breaking due to gravity was found to be at the root of many of the responses studied in vertically vibrated systems. What is the observed response in a system with a restored symmetry? Interestingly, all the observed responses have been seen in vertically shaken systems, but now they arise through essentially different mechanisms. A striking example is the presence of a stable period-doubling response, despite the negative theoretical prediction [31].

Another advantage of the present work is the wide range of time scales over which the system is studied. Most of the work done on horizontally excited systems has been limited to understanding a particular response mode, e.g., convection [3,13,27,28], fluidization [30], and other modes [31–36]. We take a different approach, studying several responses of the system on the time scales ranging from 0.1 to 20 oscillation periods. This enabled us to go beyond understanding individual responses and to discover important connections between them, most notably, the presence of a surface layer on all timescales.

These complex connections, as well as the individual responses and other results are described and discussed in Secs. III and IV, and summarized in the conclusions (Sec. V). We begin by describing the gap that opens periodically at the side walls, due to the lagging response of the material (Sec. III A). Further, we decompose the system response into components at the frequency of excitation and its subharmonics, and at zero frequency (convective flow). These responses, as well as the shearing caused by inertial forces at the top free

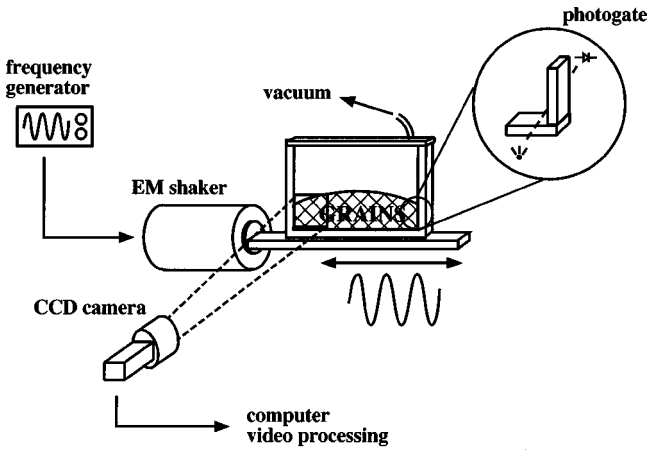

FIG. 1. Sketch of the experimental setup. An electromagnetic shaker, controlled by a frequency generator, vibrates a sled to which a rectangular container is attached. The granular material inside the container is kept under vacuum. A high-speed CCD camera is used to record the motion of the particles. These data are later analyzed by a computer. The inset shows the photogate, consisting of a light source and a photodiode, positioned at the edge of the side wall. The photogate is used to measure the duration of the gap that opens between the material and the side wall.

surface, are described in Secs. III B–III E. For both convective and harmonic response, as well as for shearing, we observe a surface layer in which the behavior of the material differs from that in the bulk (Sec. III F). Section IV discusses the properties of the surface layer (Sec. IV A), the relation of the gap to responses in the system (Sec. IV B), and also all the observed responses, including their connection to shearing (Sec. IV C–E).

II. EXPERIMENTAL SETUP AND DATA PROCESSING

A. Experimental setup

A sketch of the experimental setup is shown in Fig. 1. The apparatus consists of a rectangular container filled with poppy seeds. The sample container was constructed from acrylic, specially coated to prevent electrostatic buildup, with dimensions of length $L=200$ mm, height $H=150$ mm, and width $W=25$ mm. The poppy seeds are kidney shaped, with an average diameter of $d=0.8$ mm. Their matte surface and irregular shape facilitate visualization and prevent crystallization along the walls, while their nonabrasiveness protects the antistatic coating on the container. Unless otherwise specified, the data described in this paper pertain to a fill level $h_0=33$ mm, i.e., an aspect ratio of 0.17. The relatively small width of the system ($\approx 35d$ for poppy seeds) ensures that there are no significant variations in behavior across the cell. The lateral convection, previously described by Tennakoon, Kondic, and Behringer [28] is negligible, due to low-friction boundary conditions. During the experiments the container was kept under vacuum ($p<1$ Torr), in order to exclude the effects of any interparticle fluid. The container was mounted to a massive steel sled that was constrained to precise horizontal motion by two pairs of Teflon® guides. This construction eliminated any gap between the sled and the guides, and the 1 cm thickness of the sled did not allow any buckling that might lead to a resonance. The system was driven by a Vibration Testing Systems electromagnetic shaker. We describe the motion of the container by $x_{\mathrm{cont}}(t)=A_0\cos(\omega t+\psi_0)$, where A_0 is the amplitude of the container motion, $\omega=2\pi f$, where f is the frequency of the excitation, and ψ_0 is chosen such that phase $\psi=\omega t+\psi_0$ is zero when the side wall is at the maximum elongation in the direction away from the granular material. Any residual vertical motion of the container was determined optically to be at the same frequency and in phase with the driving of the system, with an amplitude of $\leqslant 2\%$ of that of the horizontal motion. The acceleration in the horizontal direction was measured using a PCB Piezotronics accelerometer. With this system we were able to reach accelerations of $\Gamma=10$, where $\Gamma=A_0\omega^2/g$ is the peak acceleration, normalized by $g=9.8\ \mathrm{m/s^2}$, the Earth's acceleration. The frequency range explored was 8–100 Hz. The end points of this interval were determined by experimental constraints. Below 8 Hz, the shaker could not produce an amplitude A_0 large enough to excite the system significantly. Above 100 Hz, the response of the material was too weak to be resolved. The mobilization of friction between the sled and the Teflon® guides caused a small discontinuity at the extremes of the acceleration trace, typically about 10% of the peak acceleration at $\Gamma=3$. In addition, the accelerometer could detect the impact of the granular material at the container wall. These features caused the appearance of higher harmonics, but within the measured frequency range, no other resonances were observed in the accelerometer response.

To measure the motion of the grains in the container, using either Kodak EktaPro or MotionCorder high-speed CCD cameras, we collect images at the rate of 1000 frames per second, or 30 frames per cycle at $f=33$ Hz. We choose ten evenly spaced frames per oscillation cycle and quantify the motion by calculating displacement or, equivalently, the average-velocity fields, for the time interval lapsed between a pair of frames. The algorithm for calculating the velocity fields is described below, in Sec. II B. This imaging technique allowed tracking of particles on the front or back walls of the container. To obtain the velocity fields, we processed data taken over 20 oscillation cycles. After calculating the depth profiles of various physical quantities characterizing the responses, e.g., the convection velocity or the amplitude of harmonic response, we track their dependence on Γ and f. The depth profiles were taken at a distance of $0.2L$ away from side walls. This distance was chosen because it is in the region where the convective motion of the material is horizontal, hence easy to quantify. In order to obtain satisfactory spatial resolution, only a portion of the visible surface of the material could be included in the field of view at any given time. With large filling heights and small diameter grains, we combined the data from two such fields, positioned one above the other, in order to obtain full height information. In addition, on long time scales the motion of the grains, i.e., the convection pattern, was observed over periods of up to 1000 cycles using a strobed flash that was phase locked to the driving frequency.

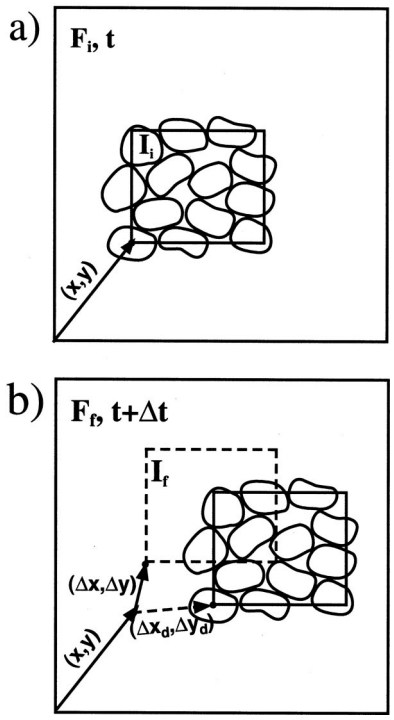

FIG. 2. The illustration of the image processing algorithm (a) F_i is an image of the system taken at time t. I_i is a rectangular area in F_i, of given dimensions and originating at (x,y). The grains contained in I_i form a cluster whose motion we track. (b) F_f is an image of the system taken at time $t+\Delta t$. Over the time interval Δt, the cluster contained in I_i is displaced by $(\Delta x_d,\Delta y_d)$. I_f is a rectangular area in F_f of the same size as I_i, originating in $(x+\Delta x,y+\Delta y)$, where $(\Delta x,\Delta y)$ is varied. The similarity of I_i and I_f for various $(\Delta x,\Delta y)$ is quantified by function $C(\Delta x,\Delta y,\Delta t)$, defined in Eq. (1). When $(\Delta x,\Delta y)=(\Delta x_d,\Delta y_d)$, $C(\Delta x,\Delta y,\Delta t)$ has a sharp minimum. The mean velocity of the grains over Δt is $(\langle v_x\rangle,\langle v_y\rangle)=(\Delta x_d,\Delta y_d)/\Delta t$.

At the vertical side boundary of the system, a gap opens between the material and the vertical wall during a fraction of each cycle, due to the lagging response of the material. We observe this gap using a video camera to determine its width and maximum depth δ_g. In order to measure its duration τ_g, we mounted a photogate at the edge of the side wall of the container. When the gap is closed, no light can pass through to the photodiode, and when the gap opens, light passes through. The signal from the photogate was captured by a Pentium II computer using a National Instruments A/D card and Labview software. Up to 200 cycles were captured in a single measurement, with a typical time resolution of $0.001T$.

B. Video processing algorithm

The video processing algorithm is illustrated in Fig. 2. After taking a high-speed movie, we track the motion of grains between two frames, F_i (Fig. 2a) and F_f (Fig. 2b), captured at times t and $t+\Delta t$, respectively. Over time Δt, a $3d\times 3d$ rectangular area I_i, originating at (x,y) in F_i, is displaced by $(\Delta x_d,\Delta y_d)$. This displacement can be found by comparing I_i to different $3d\times 3d$ areas I_f, originating at $(x+\Delta x,y+\Delta y)$ in F_f, where $(\Delta x,\Delta y)$ is varied. We evaluate how similar I_i and I_f are by calculating $C(\Delta x,\Delta y,\Delta t)$,

$$C(\Delta x,\Delta y,\Delta t)=\langle (I_i-I_f)^2\rangle/(\langle I_i\rangle\langle I_f\rangle). \tag{1}$$

We choose this function rather than the more usual correlation function $\langle I_1 I_f\rangle/(\langle I_i\rangle\langle I_f\rangle)$ because we obtain a better signal-to-noise ratio. For random packing, only for $(\Delta x,\Delta y)=(\Delta x_d,\Delta y_d)$, I_i and I_f are almost identical and $C(\Delta x_d,\Delta y_d,\Delta t)$ has a sharp minimum. Thus we measure

$$\langle \mathbf{v}\rangle(x,y,t)=(\langle v_x\rangle,\langle v_y\rangle)=(\Delta x_d,\Delta y_d)/\Delta t \tag{2}$$

as the velocity vector of the material at position (x,y), at time t. By choosing different values for Δt, we can calculate the mean velocity of the material on time scales ranging from 0.1 to 20 oscillation periods.

By comparing $3d\times 3d$ areas in frames F_i and F_f, this computer algorithm effectively tracks particle clusters, rather than particles themselves. Consequently, it allows the use of images of much lower resolution than would be needed for a successful single particle-tracking algorithm. This significantly speeds up data acquisition and processing relative to conventional particle tracking, allowing a larger dynamical range, and a larger field of view. This method is only applicable to dense, laminar flows, in which the rearrangements of the particles are rare events. In rapid flows, which exist at the top and side boundaries of the system, the particle clusters rearrange rapidly. $C(\Delta x_d,\Delta y_d,\Delta t)$ has multiple random minima, and the algorithm fails, yielding large amplitude random noise.

III. RESULTS

A. Gap

Figure 3 shows the behavior of the system at the side wall throughout an excitation cycle. During part of each cycle, the granular material is pushed by the side wall towards the center of the container [Fig. 3(a)]. After the wall retracts, the material lags behind it and a gap opens between them [Fig. 3(b)]. Initially, the gap opens uniformly in height, but soon becomes wider near the top surface. After the container wall reverses its direction at the beginning of the following cycle [Fig. 3(c)] the gap closes nonuniformly from the bottom up [Fig. 3(d)]. The temporal sequence of events with respect to container motion is shown in Fig. 3(e). The shaded areas in [Fig. 3(e)] correspond to the intervals during which any part of the gap is open.

In Figure 3, the peak excitation acceleration Γ is sufficiently large that the maximum depth of the gap δ_g is equal to the full depth of the system, i.e., the gap is fully open. At lower Γ, δ_g is smaller, (as shown in Fig. 5), and the gap consists of an upper, wider region and a narrow tail, penetrating deep into the material. This is more pronounced at lower frequencies, while at higher f there is progressively less distinction between these two regions.

The maximum gap depth within a cycle, δ_g, is observed optically by using a high-speed video camera. We define δ_g with respect to the nominal fill level h_0, rather than the dynamically changing instantaneous surface level during vi-

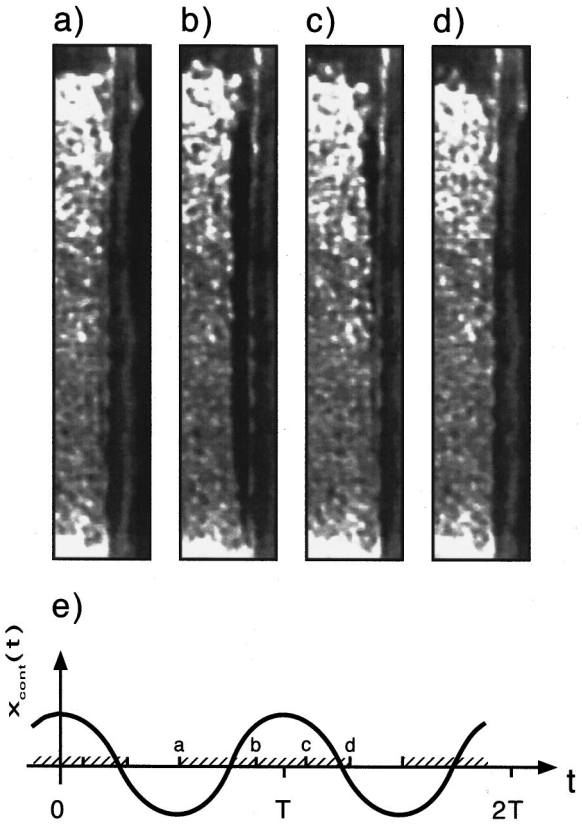

FIG. 3. A snapshot of the vertical boundary at four different phases in the cycle: (a) just before the gap begins to open; (b) at full extension of the gap; (c) when gap is partially closed; (d) just after the gap closes fully; (e) The time-space diagram shows the position of the container wall, x_{cont}, over two oscillation cycles. The gap is open during the shaded time intervals. The letters on the diagram indicate moments in cycle at which the corresponding snapshots were taken. The images were taken at $\Gamma = 3.4$.

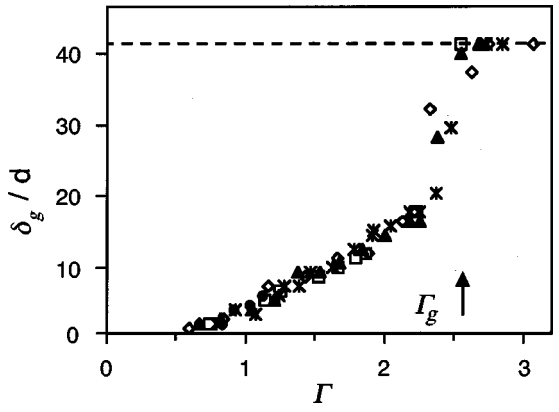

FIG. 4. The dependence of maximum gap depth δ_g on Γ. The data taken at 8 Hz (●), 15 Hz (□), 25 Hz (▲), 33 Hz (◇) and 50 Hz (∗) overlap, indicating no frequency dependence. The gradual increase has an onset at $\Gamma \approx 0.5$. The sharp jump at Γ_g brings δ_g equal to the full filling height $h_0 = 41d$. The size of the symbols corresponds to the error bars of the measurement.

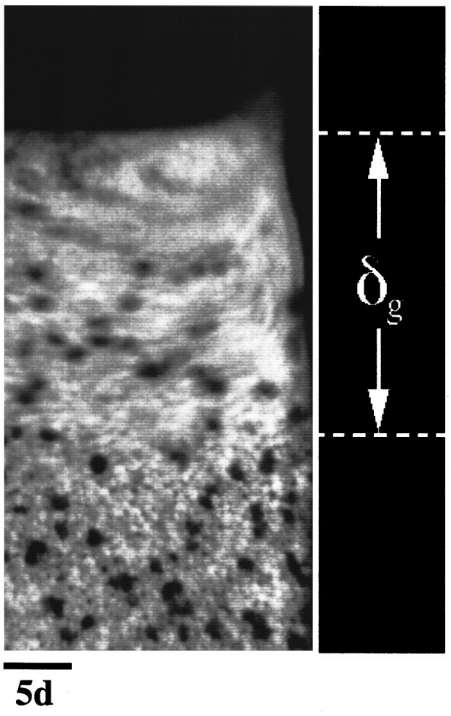

FIG. 5. A many-cycle superposition photograph of the vertical boundary of the system, taken at $\Gamma = 2$, $f = 20$ Hz and $h_0 = 50$ mm. The images were taken at the phase of oscillation at which the gap is at maximum depth, denoted by δ_g. The blurring in the upper region results from convecting particles, while the sharp lower portion of the image indicates zero convective motion.

bration. Its dependence on Γ is shown in Fig. 4. One can clearly distinguish two regimes. For small Γ, the gap opens at an onset acceleration amplitude $\Gamma \approx 0.5$. In this regime, δ_g grows steadily until Γ_g, where it suddenly jumps to the full depth of the container, indicated by the dashed line at $h_0 = 41d$. Beyond Γ_g we identify the second regime, in which the gap extends to the bottom of the container and remains constant with increasing Γ. Data, taken at frequencies between 8 and 50 Hz, overlap, indicating no frequency dependence in this range.

Figure 5 is a long-exposure photograph of the vertical boundary of the system, taken at $\Gamma = 2$, $f = 20$ Hz, and $h_0 = 50$ mm, under a phase-locked strobed light, at the phase of oscillation at which the gap reaches the maximum depth. The blurring in the upper region is a result of the convective motion of the grains. The sharp lower part of the image corresponds to the nonconvecting region, in which there is no relative grain motion. The maximum depth of the gap δ_g coincides with the depth of the transition between convecting and nonconvecting region—it equals the convection fluidization depth in the system.

As the gap closes from the bottom up, we define τ_g as the interval during which the gap is open *at the height of measurement* (Fig. 6). It is measured 20–25 mm above the container bottom, where period doubling in the material was most pronounced. τ_g grows nonlinearly with Γ and undergoes a period doubling bifurcation at $\Gamma' = 3.7$, and a period quadrupling bifurcation at $\Gamma'' = 5.9$. Figure 6 shows the av-

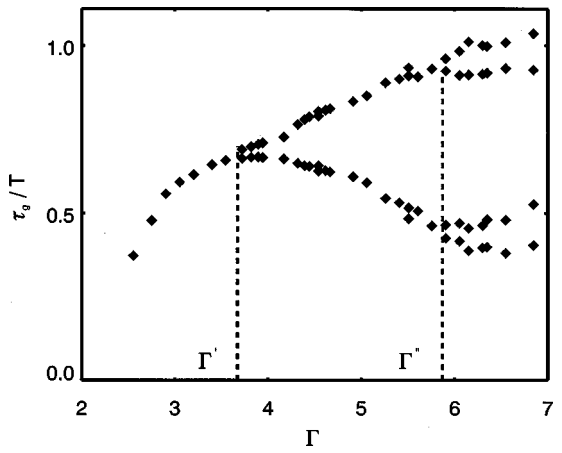

FIG. 6. The dependence of gap duration τ_g on Γ. τ_g undergoes a period-doubling bifurcation at $\Gamma' = 3.7$, and a period-quadrupling bifurcation at $\Gamma'' = 5.9$.

erage values for τ_g in these regimes. The highest branch of τ_g on Fig. 6 grows larger than 1 at $\Gamma = 6$, indicating gap duration longer than a full oscillation period. The low values of τ_g below $\Gamma = 2.5$ could not be measured reliably. While period doubling is very stable, the period quadrupling was maintained during only 30–50 % of the observation time. We found no evidence of hysteresis at the period doubling bifurcation, and only a weak frequency dependence of Γ'. Over the 18–50 Hz frequency range, Γ' increases by only 20%, from 3.5 to 4.2.

B. Convection

Convection, the long-range transport of the material throughout the container, is the slowest mode in the system. The detailed dependence of the convection pattern, i.e., of the shape and number of the convection rolls, on the boundary conditions is described elsewhere [13]. In the given setup, the convection is conducted in two symmetrically positioned quasi-2D convection rolls (Fig. 7), with the direction such that transport of the material is downward at the walls and upward in the center of the container. At low Γ, the fluidization of the system is only as deep as the gap depth δ_g (Fig. 5) and the rolls exist only above δ_g. Once the material is fully fluidized and the rolls reach the bottom of the container, their shape does not evolve with increasing Γ [13].

Figures 8(b), (c), and (e) show the velocity fields on the front surface of the system, in the region outlined in Fig. 8(a). The velocity fields are measured as explained in Sec. II B, on varying time scales, i.e., averaged over a varying time interval Δt. These fields differ greatly in intensity and shape. In particular, Fig. 8(b) shows the convection velocity field, in which a convection roll is easily distinguishable.

We quantify convection by calculating the depth profile of its velocity field, at distance $0.2L$ [dashed line in Fig. 8(b)] away from the wall, where it is mainly horizontal. We track the motion of the particles over four cycles, with time resolution of $T/10$. The horizontal motion is fit to a harmonic function of time, with a linear term accounting for horizontal convective velocity v_x. From this depth profile, shown in

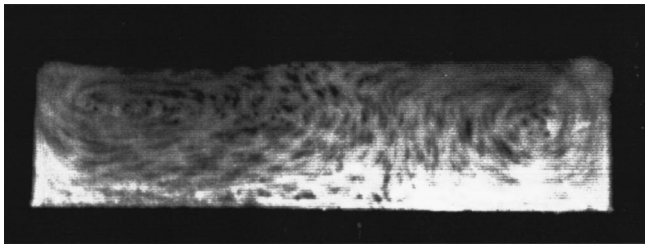

FIG. 7. A many-cycle superposition photograph of the front container wall reveals two symmetrically positioned convection rolls. A phase-locked strobe light is used so that each frame is taken at the same phase in the cycle. The streaking is due to the motion of the tracer particles (dark colored poppy seeds) mixed with the material (light colored poppy seeds). The image is taken at $\Gamma = 6$ and $h_0 = 50$ mm, and shows the entire system.

Fig. 9(a) (solid line) for $f = 33$ Hz and $\Gamma = 2.9$, one can distinguish two regions: The bulk of the material convects slowly away from the side wall, with an approximately constant negative velocity. Above it one observes a surface layer, convecting toward the side wall (positive velocities). Between the bulk and the surface layer, there is a crossover region in which v_x sharply decreases with depth. The dashed line on Fig. 9(a) represents $-\partial v_x / \partial D$, whose maximum absolute value determines the depth of the crossover region, or, the characteristic depth for convection D_c. Its dependence on Γ is shown on Fig. 10 (triangles). It grows with Γ up to $\Gamma = 3$, and then levels off to a constant value of $\approx 16d$.

C. Harmonic response

The driving at frequency f produces a response at the same frequency. We track the motion of the grains on the front surface over four cycles and on the time scale of $T/10$. Below $\Gamma = 4.5$, outside of a narrow boundary zone at the side walls of the cell, the motion of the grains is approximately sinusoidal, with a well-defined amplitude and phase. Above $\Gamma = 4.5$ there is a strong subharmonic component at half the excitation frequency, superimposed on the harmonic response. Using the image processing software, we can separate the two harmonics, fitting the motion of the grains first to a harmonic response (with convection accounted for by a term linear in time) and then fitting the residual response to the half-frequency harmonic.

The harmonic behavior can be seen in Fig. 11. Figure 11(a) shows the time and height dependences of the horizontal position of a particle, at the distance $0.2L$ away from the side wall, at $f = 33$ Hz and $\Gamma = 4.5$. The vertical axis corresponds to the height above the container bottom, while the horizontal axis shows time, in oscillation periods T. The x coordinate of the particle is shown on a brightness scale: the bright regions correspond to positive displacements around the mean value (in the direction toward the side wall), while the dark regions correspond to negative ones. In Fig. 11(b), the time dependence of a particle's position at three different heights above the bottom is isolated. The vertical scale in Fig. 11(b) measures the horizontal displacement of the particles around the mean value, denoted by the dashed horizontal lines. These lines are offset to indicate the heights at

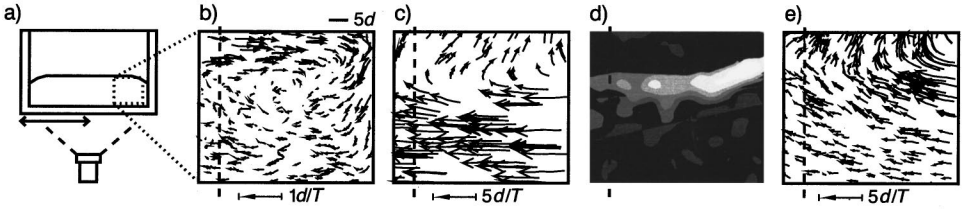

FIG. 8. (a) A sketch of the system. The dotted square outlines the region shown in (b)–(e). After analyzing the particle motion recorded by the high-speed CCD camera, we obtain the velocity fields at various time scales. (b) The convection velocity field, as measured over $20T$, is shown. (c) The velocity field at the time scale of $T/2$, resulting from the harmonic response of the system, is shown. (d) The shear field Q, as defined by Eq. (3) and calculated from velocity data obtained on $T/10$ time scale, is shown on a brightness scale, with bright corresponding to high values of Q; (e) The period-doubling vector field, significant on time scales of T, is shown. Note that, when observed at different time scales, the velocity fields differ significantly in shape and intensity. The dashed vertical lines are positioned at the distance $0.2L$ away from the side wall, and mark the position at which the depth profiles of various physical quantities are taken.

which the particle displacements were measured, in accordance with the height axis in Fig. 11(a). From Figs. 11(a) and (b) one can distinguish two regions in the material. In the bulk, there is very pronounced horizontal harmonic motion of the particles. Above the bulk, there is a surface layer, in which the horizontal motion of the grains has a much smaller amplitude and a large phase lag with respect to the bulk. The slight slope in the time traces in Fig. 11(b) indicates convective motion. Note that convection is very slow, compared to the harmonic oscillations—one can observe it readily only in the surface layer where it is relatively strong, and the harmonic response is very weak. It is also possible to observe the period-doubling contribution through the alternating high and low amplitudes of motion in the surface layer.

Figures 11(c) and (d) show the analogous information for the vertical displacements of the particles. While there is no clear distinction between the bulk and a surface layer, the vertical motion is more pronounced near the surface. Also, for vertical motion, the sinusoidal time dependence is a good approximation near the surface, but not in the bulk. The period doubling is clearly seen in the surface layer time trace. There is no visible contribution due to convection.

The harmonic motion of the material is characterized by its amplitude A_h and phase offset ϕ_h at every point, obtained by fitting the horizontal position of a particle to a sinusoidal function of time (with a linear term accounting for convection). The depth profiles of A_h and ϕ_h at $0.2L$ away from the side wall are shown on Figs. 9(b) (solid line) and 9(c), respectively. The amplitude deep in the bulk is constant and at $\Gamma<3$ scales with the amplitude of the container motion. Above $\Gamma=3$, A_h does not change value with increasing Γ. In a well-defined surface layer, the amplitude is much lower in value. In the laboratory frame of reference, the surface layer appears almost motionless, while the bulk moves with a large amplitude. The dashed line shows $\partial A_h/\partial D$, the depth gradient of A_h. Its peak locates the position of the region of growing A_h, which we call the characteristic depth for harmonic motion, D_h. The dependence of D_h on Γ is shown in Fig. 10 (diamonds). D_h grows with Γ up to $\Gamma=3$, after which it levels off to a constant value $\approx 16d$. Note that its Γ dependence is the same as the dependence of the characteristic depth for convection, defined above.

The depth profile of the phase of harmonic response ϕ_h is shown in Fig. 9(c). It does not show sharp features at the crossover from the bulk to the surface region. Rather, it remains approximately constant in the bulk, increasing throughout the transition region, towards the surface layer. The phase lag grows slowly with peak acceleration, and is higher for deeper beds. At $h_0=95$ mm, we observed phase lags of over 360°. The value of ϕ_h deep in the bulk is exactly zero for small Γ, since the material is forced to track the motion of the container. At higher Γ, however, the material slips on the smooth container bottom, which produces a gap between it and the side wall, and an offset in the bulk phase values. This offset value has been subtracted from the ϕ_h profile shown in Fig. 9(c).

D. Shear

When the side walls push the material in front of them in their motion towards the cell center, their action is only at the boundary of the material. Because of inertia of the particles, strong shearing stresses form at the top free surface, and the material fails along a plane running at a constant depth beneath the surface. This creates a localized shear band, which separates the strongly moving bulk of the material from a more stationary surface layer. Close to the side walls, the shear plane curves upwards, ending in the upper corners of the system.

While the isotropic part of the shear tensor describes dilation in the material, the shearing can be quantified by the amplitude Q of its volume-conserving part.[1] For the 2D velocity fields that we observe at the front surface, both inside and outside of the shear band, this scalar quantity is obtained by a simple expression in Eq. (3). We calculate the shear tensor from the short-time velocity field at a time resolution of $T/10$.

$$Q=\frac{1}{2}\left[\left(\frac{\partial v_x}{\partial x}-\frac{\partial v_y}{\partial y}\right)^2+\left(\frac{\partial v_x}{\partial y}+\frac{\partial v_y}{\partial x}\right)^2\right]^{1/2}. \qquad (3)$$

[1]The n-dimensional shear tensor $\nu_{ij}=\frac{1}{2}(\partial_i\nu_j+\partial_i\nu_j)$ can be represented as the sum of two terms, $\nu_{ij}=(1/n)\,\delta_{ij}\nu_{kk}+(\nu_{ij}-(1/n)\,\delta_{ij}\nu_{kk})$, the first one describing the hydrostatic compression, and the second describing the volume-conserving, or pure, shear deformations. The absolute value Q of the second term equals the square root of the sum of squares of its elements. In two dimensions, it reduces to Eq. (3).

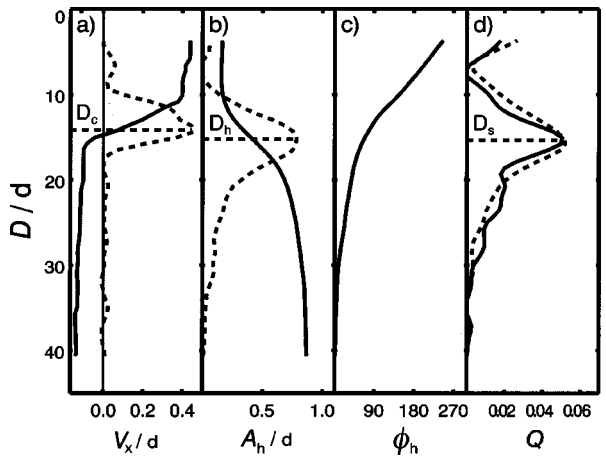

FIG. 9. The depth profiles of the physical quantities used to characterize the motion on different time scales. (a) The depth profile of the horizontal convection velocity, v_x (solid line) is shown in units of 1/cycle. Its negative depth gradient, $-\partial v_x/\partial D$ (dashed line, on an arbitrary scale), is also shown. The peak in the depth gradient determines the characteristic depth for convection D_c. (b) The depth profile of the amplitude of the harmonic response, A_h (solid line), and its depth gradient, $\partial A_h/\partial D$ (dashed line, arbitrary scale), are shown. The peak in the depth gradient determines the characteristic depth for harmonic response D_h. (c) The depth profile of the phase lag of the harmonic response ϕ_h is shown in degrees of angle. It is offset so that the phase lag deep in the bulk is zero. (d) The depth profile of Q [Eq. (3), solid line] at the maximizing phase within the cycle is shown, in units of 1/cycle. The peak in the depth profile of Q determines the characteristic depth for shear D_s. The noise floor of 0.017/cycle, determined from the profiles measured at low Γ, has been subtracted. The dashed line shows the contribution to shear from the horizontal harmonic motion, as calculated from A_h and ϕ_h. All the depth profiles were measured at $0.2L$ away from the side wall, at $f=33$ Hz and $\Gamma=2.9$.

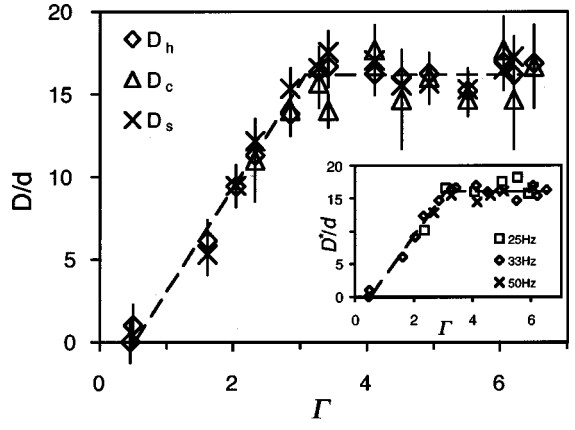

FIG. 10. The dependence of the characteristic depths D_c, D_h, and D_s on Γ. Note that, within the experimental accuracy, they all trace the same curve. The dashed line is a fit to the average of their values D^*, linear up to $\Gamma=3$, and constant thereafter. The inset shows the values of D^* for three different frequencies, 25, 33, and 50 Hz. There is no observable frequency dependence. The dashed line is the same as in the main figure, and is shown for reference.

Figure 8(d) shows a snapshot of Q at $\psi=108°$, the phase at which it is maximized. The bright band corresponding to the localized shear band is easily observed. Away from the boundary and below the period-doubling transition, Q preserves the symmetry of the excitation: at any moment t, it has the same values as at the moment $t-T/2$. We construct the depth profile of Q at the distance $0.2L$ away from the side wall and at the maximizing phase, and show it in Fig. 9(d) (solid line). The depth at which Q reaches the maximum value $Q_{\max}$ determines the depth of the shear band, or, the characteristic depth for shearing D_s. The Γ dependence of D_s is shown in Fig. 10. Note that it has the same dependence as the characteristic depths for convection and harmonic response, defined earlier.

The gradients in the amplitude and phase of harmonic motion give rise to a shearing contribution of the harmonic response. Using A_h and ϕ_h data and Eq. (3), we calculate this contribution and plot it in Fig. 9(d) (dashed line) for the same position and phase of oscillation at which Q was measured. Surprisingly, within the resolution of our experiment, it coincides with the directly measured shear values Q. Figure 12 plots $Q_{\max}$ at various Γ vs the difference, ΔA_h, of the corresponding bulk and surface layer harmonic amplitudes, for three different frequencies. Although there is significant scatter in data taken at a particular frequency, overall linear scaling of $Q_{\max}$ with ΔA_h is present. The open symbols correspond to the data taken above $\Gamma=4.5$, at which value the strong period-doubling contribution is first observed in the depth profiles of Q. (While the period-doubling onset is well below this value, for lower accelerations its contribution is negligible at the distance at which the depth profiles of Q were taken.) Above the period-doubling transition, the material does not have time to fully relax after each shearing, but is alternately sheared in the relaxed and a dilated state, and the shear band exhibits period doubling. In this case, Q was calculated only in the cycle in which the material was relaxed before the shearing.

E. Subharmonic responses

We have already described the period doubling at the system boundary, as observed via the bifurcation in the gap lifetime τ_g (Fig. 6). However, this is just a signature of the period doubling deeper inside the system: after accounting for the harmonic and convective responses in the velocity fields, a period-doubling component remains above $\Gamma=3.5$. By fitting this remaining response to a harmonic at half the excitation frequency, we obtained the amplitude and phase of the period doubling. Such an approach, though, decouples the horizontal and vertical components of motion, whose relationship is essential for understanding the mechanism driving the period doubling.

Instead, we quantified the period doubling by defining the period doubling vector field, as follows. Below the period-doubling bifurcation, at the phase of oscillation of, e.g., $\psi=0$, a particle is found at the same (x,y) position in each oscillation cycle (neglecting convection). Above the bifurcation, at the same phase of oscillation ψ, the particle alternates between two different positions from one cycle to the next.

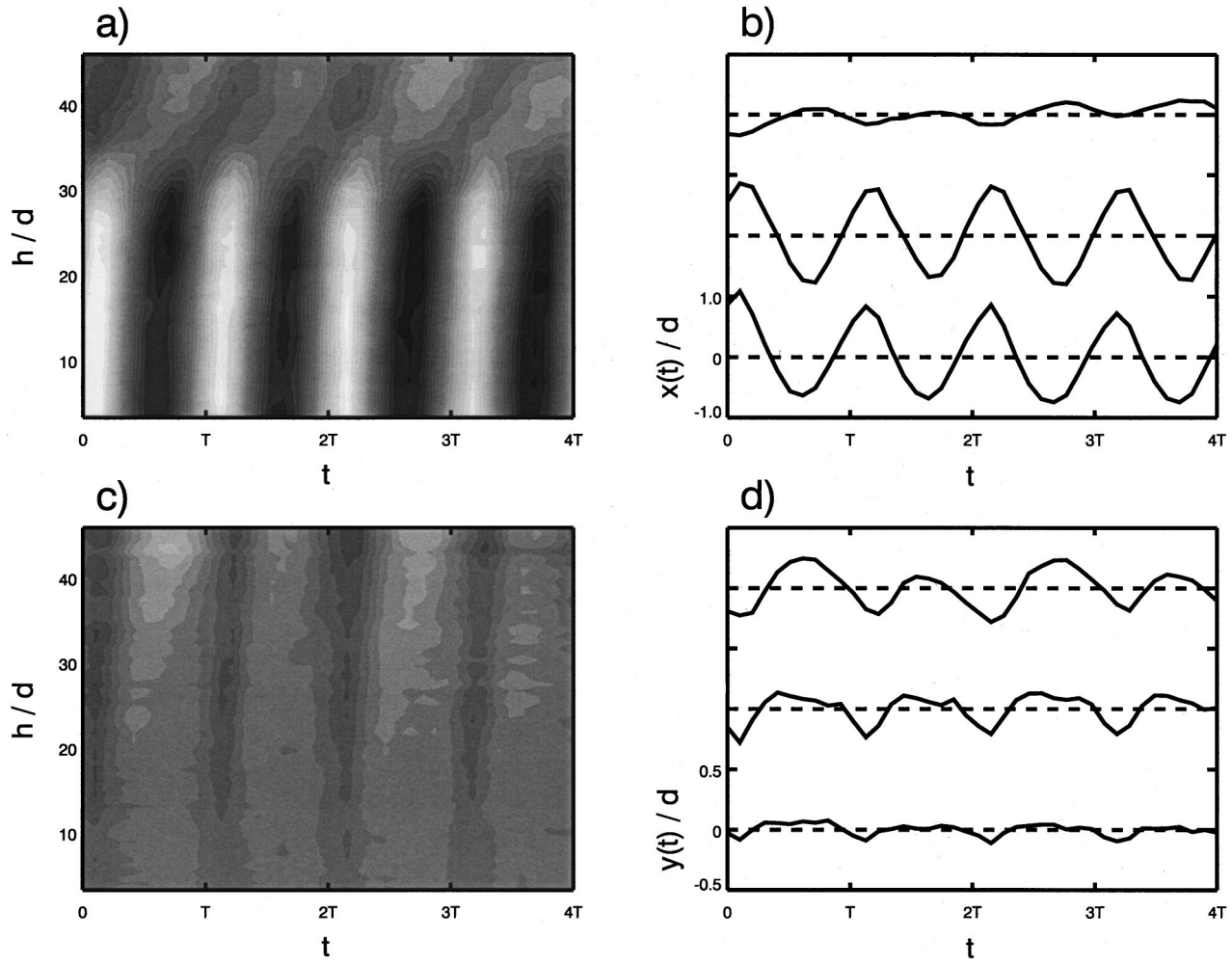

FIG. 11. The time and height dependence of a particle's coordinates on the container front, at a distance $0.2L$ away from the side wall, for $f=33$ Hz and $\Gamma=4.5$. (a) The time and height dependence of the x (horizontal) coordinate. The vertical axis denotes height above the container bottom. The horizontal axis denotes time in oscillation periods T. The brightness of the image represents the value of the x coordinate on a brightness scale, with bright corresponding to positive values (closer to the side wall), and dark corresponding to negative values (further away from the side wall). (b) The time traces of a particle's x coordinate are shown for three different heights above container bottom. The dashed horizontal lines mark these heights according to the vertical axis on (a). They double as the mean value for the time traces. The horizontal scale represents time in oscillation periods, while the vertical measures displacement around the mean value. (c) The time and height dependence of a particle's y (vertical) coordinates, analogous to (a). The arbitrary brightness scale is identical to the scale used in (a). (d) The time traces of vertical displacements, analogous to (c).

The vector difference between these two positions we call the period-doubling vector. A representative period-doubling vector field, calculated at $\psi=0$, is shown in Fig. 8(e). It is largely horizontal, except near the surface, where it acquires a vertical component. Note that this vector is defined with respect to the phase ψ of the excitation, which is unique for the whole system.

The period doubling is strongest in the upper corners of the systems. In fact, at low ($\Gamma\approx3.5$) accelerations, it is completely localized to these corners: by stirring the material with a stick, we were able to perturb the motion of the material in one of the corners, changing the sign of the period-doubling field, (i.e., changing the order of alternating (x,y) positions of a particle at $\psi=0$), without changing its sign at the opposite wall. Thus, the period doubling is a local effect—not the response of the body as a whole.

Comparing Figs. 8(d) and (e) one can see that both an inclined shear band and a pronounced period doubling are local features in the upper corner of the system. The corner regions are zoomed in on in Fig. 13(a), in which the arrows represent the period doubling field, and the dashed line the position of the shear band. The period doubling field is predominantly horizontal below the shear band, and vertical above it. This is also true away from the corners.

We observed period quadrupling in the velocity fields at $\Gamma>6$, and also by measuring the duration of the gap, τ_g (Fig. 6), and by observing the shape of the gap using the high-speed camera.

F. Surface layer

In the previous chapters, we defined the characteristic depths for convection D_c, harmonic D_h, and shearing re-

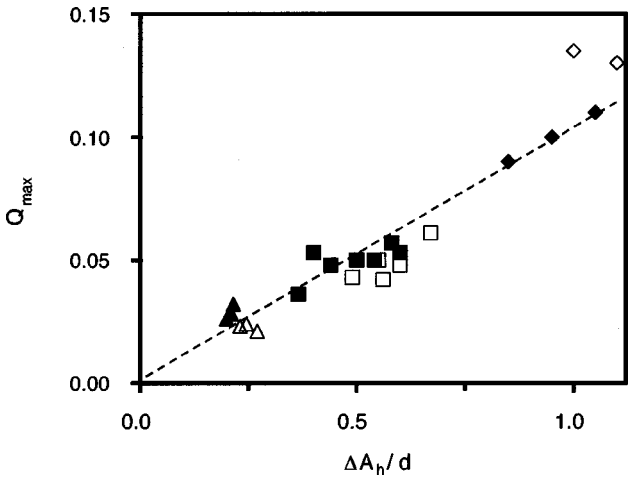

FIG. 12. The maximum shear values $Q_{\max}$ (units of 1/cycle) scale linearly with the difference between the bulk and surface amplitudes of horizontal harmonic motion, ΔA_h. The three symbols correspond to $f=25$ Hz (diamonds), 33 Hz (squares), and 50 Hz (triangles). The dashed line is a guide to the eye. The open symbols represent data taken above $\Gamma=4.5$, at which values there is a contribution from period doubling.

sponse D_s (Fig. 9). For all of these responses, one can distinguish a surface layer of different character from the bulk of the material. At the longest time scales, oppositely convecting parts of the convection roll are separated at the characteristic depth for convection D_c. At intermediate time scales, the surface layer shows a different fluidization pattern from the bulk, moving with a smaller amplitude and a nonconstant phase. Finally, at the shortest time scales, D_s measures the depth of the localized shear band forming between the oppositely moving surface layer and bulk. The dependence of characteristic depths D_c, D_h, and D_s on Γ is plotted in Fig. 10. Above $\Gamma=6$, the data were too noisy to process using our image processing software. Below $\Gamma=2$, as the convection profiles were not fully developed, D_c was not well defined. The D_s data point at $\Gamma=0.5$ was not measured by fitting the response of the material to a harmonic function, but represents the measured onset of fluidization.

Within experimental accuracy, all characteristic depths essentially trace the same curve. Thus it is justified to define the characteristic depth D^* as their mean value. D^* grows linearly from the fluidization onset at $\Gamma=0.5$ up to $\Gamma^*=3$, at which value it levels off and remains constant at $\approx 16d$. The inset shows the measured values of D^* for three different frequencies. Within the given experimental range (25–50 Hz), no frequency dependence was observed.

IV. DISCUSSION

A. Surface layer

In the observed responses, we find a well-defined separation of the system into two layers of different character—a surface layer's motion is decoupled from the motion of the bulk of the material. This is true for convection, harmonic response, and shearing. The period-doubling vector also changes direction in the surface region (above the shear band). The identical depths of the surface layers observed for different responses (Fig. 10) lead to the conclusion that a single surface layer is formed in the system, well defined and maintained on all time scales, and justify the definition of D^* as a measure of its depth. This surface layer is likely due to the open boundary condition at the top of the container, as it is separated from the bulk by the shear band, at depth D^*. It is through this surface layer that the fluidization of the system is initiated. Although the bulk apparently moves with a larger amplitude, it only passively tracks the motion of the container.

A similar surface layer was previously observed by Tennakoon, Kondic, and Behringer by observing yet another response mode in a horizontally vibrated system: the lateral convection [28]. The experiments agree in that the fluidization of the system is initiated at the top free surface, and propagates into the bulk with increasing Γ. Another experiment by Ristow, Straßburger, and Rehberg [30] also finds fluidization initiated at the surface, and reports onset values of $\Gamma=0.1$ and $\Gamma=0.8$. Also, Pouliquen, Nicolas, and Weidman [33] achieve crystallization of glass spheres under low-amplitude horizontal vibrations by continuously adding small amounts of material at the surface: the body of the crystal remains undisturbed, while the surface particles are fluidized just enough to form additional crystal layers. Their onset for crystallization at $\Gamma=0.5$, corresponds to our fluidization onset value of 0.5. Moreover, exploring accelerations up to $\Gamma=2$ they observe $n_{\ell}=0-6$ fluidized particle layers, in approximate agreement with our $\partial D^*/\partial\Gamma=6d$.

B. Gap

We find that, just like the surface layer, the gap is also related to all the system responses. For example, the gap duration τ_g exhibits period doubling. Further, δ_g is equal to the convective fluidization depth in the system (Fig. 5), consistent with convection being driven by the avalanching of the grains into the open gap [27,28]. But, δ_g is also equal to the depth of fluidization due to the harmonic response. Rather than being a result of the dilation and compression of the material at the boundary, the gap is due to the phase lag and decreasing amplitude of the fluidized material in the surface layer. Below δ_g, the material essentially tracks the motion of the container, moving as a solid body. As the constant amplitude and phase do not give rise to shear, and at $\Gamma<\Gamma_g$ there is no period doubling, δ_g is actually the total fluidization depth of the system. The fact that both δ_g and the fluidization of the system have an onset at $\Gamma=0.5$ is consistent with this statement.

This should not be taken as implying that the sudden jump in δ_g at Γ_g (Fig. 4) is a signature of some dynamical transition of the system to the fully fluidized state. The lower narrow extension of the gap visible in Fig. 3(c) is first observable only at values close to Γ_g. At lower peak accelerations only the wider, upper part of the gap can be resolved. The jump thus results from the specific gap shape, which itself is due to the properties of the amplitude and phase of the harmonic response.

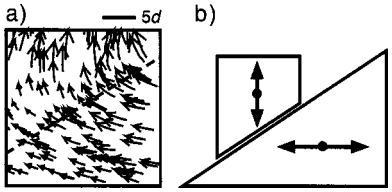

FIG. 13. (a) The arrows represent the period-doubling vector field in the upper corner region of the system. The dashed line shows the position of the shear band in the same region. The period doubling motion is horizontal below the shear band and vertical above it. (b) The two-body model for motion in the upper corner of the system is shown schematically. The material below the shear band is constrained to horizontal, and the material above it to vertical motion. The shear band thus acts as an inclined plane, transforming horizontal into vertical motion. Gravity couples to vertical motion, giving rise to period doubling.

In addition, the Γ dependence of a number of physical quantities in the system is coupled to the Γ dependence of δ_g. For example, the depth D^* of the surface layer grows linearly up to the value of $\Gamma^*=3$, after which it levels off and remains constant (Fig. 10). Above Γ^* there is also no change in A_h, as apparently the phase lag of the bulk and the growing gap width adjust accordingly. Interestingly, it is approximately at this value of Γ that the gap reaches the bottom of the container, and thus δ_g remains constant, too (Fig. 4). Moreover, we find that once the gap has reached the bottom of the container, the convection pattern does not change with increasing Γ [13].

C. Harmonic response: Relation on to shear

The depth of the shear band D_s coincides with D_h, the depth of the region of high amplitude decay (Fig. 10) This points to high dissipation in the shear region—not surprising, as one would expect increased friction or collisions there. The dense flow suggests that dissipation is caused by increased rubbing between seeds. Further, although there are small deviations at higher Γ due to period doubling and dilation in the vertical direction, at small accelerations all of the shear can be accounted for by the gradients in harmonic response. This means that there are no faster processes contributing to shearing, even though in granular materials, shear is often likened to material failure. This result is further supported by the observation that for $\Gamma<4.5$ the maximum shear value $Q_{\max}$ is proportional to ΔA_h, the difference between the horizontal harmonic amplitude in bulk and surface layer (Fig. 12), and that shear, like the harmonic response, preserves the symmetry of excitation. Thus, while, on one hand, the energy dissipation in the shear band produces harmonic amplitude decay and its observed depth profile, on the other, the specific shape of the harmonic response determines the strength of the shearing.

D. Convective response: Relation to shear

While it is intuitively clear that shear may arise from gradients in A_h or ϕ_h, the coincidence of D_c and D_s, the depth of shear band, is more puzzling. Naively, one might assume that convection results from material displacements due to shearing, but we find that shear action is equal and opposite during first and second halves of the cycle. Still, it is possible that convection is produced by small asymmetries in the leftward and rightward shearing, brought about by differences in action of the closer or of the farther side wall, or simply by material not relaxing fully between shearings, i.e., at high enough driving.

The current literature, however, cites the avalanching of the material at the side walls as the driving mechanism for convection [13,28]. Avalanching does break the symmetry of motion by accumulating material in the gap during a part of each cycle, and hence can give rise to convection. But with such a mechanism, there is no explanation of why the crossover in convective motion, at D_c, coincides with D_s and D_h. Can that model be reconciled with the present findings? Yes, by taking into account the differences in A_h between the surface layer and the bulk: as the bulk, with a large A_h, is pushed away further by the walls, the surface layer, that had not moved as much, will disproportionately avalanche into the gap.

Of course, the above discussion applies to the case in which convection is conducted in two convection rolls (Fig. 7). It is known, however, that the convection pattern is determined by the boundary conditions and container dimensions, and that additional rolls can appear, which may have the direction opposite to the direction of rolls observed in this experiment [13]. It is unclear whether, under such conditions, one would still observe coincidence of D_s and D_c.

It is tempting to try to draw a parallel between the convection induced by vertical and by horizontal vibrations. In both cases, it is induced by asymmetries in the shearing and motion paralel to driving, due to the changing material pressure in one, and to avalanching in the other geometry [13,28]. But, there is a significant difference between the two cases: while in vertically vibrated systems the shear is located at the boundary of the system and coincides with the maximum speed of convection [3,4], in the present system the shear band is induced deeper in the system and approximately coincides with the stagnation point of convection (Fig. 9). This may be due to the fact that the frictional forces act at the boundary only, while the inertial forces act throughout the volume of the system. But, it could also be due to the difference between interaction with a closed and an open boundary at which the material is free to expand upon agitation. More research is needed in order to answer this question precisely.

E. Period doubling: Relation to shear

Besides convection, another symmetry-breaking response arises in a horizontally vibrated granular material—the period-doubling response. This response has been observed and extensively studied in vertically excited granular systems [37–41]. In these systems, it is well understood in terms of an inelastic bouncing ball model [37,40,42,43] which essentially treats the granular system as a single body. However, the origin of period doubling in horizontally vibrated systems is puzzling: the extension of the bouncing ball model to the horizontal geometry fails to predict it [31]. The model does predict period two orbits for certain geometrical condi-

tions, but these orbits are realized by the body colliding with each wall only every other cycle ($\tau_g \equiv 2T$), while we observe period doubling behavior already for $\tau_g = 0.7T$ (Fig. 6). In addition, such long trajectories are unphysical, as in the experiment the material contacts the wall in every oscillation cycle, both before and after the period doubling bifurcation. Most importantly, while the inelastic bouncing-ball model describes the motion of the system as a whole, we find that in horizontally excited systems, period doubling is localized and a signature of internal degrees of freedom [14].

In order to explain the presence of the subharmonic responses, we model the motion in the upper corners of the system by using a simple two-body model [Fig. 13(b)]. While the material in the bulk (below the shear band) is forced to follow the container motion, and is thus confined to the horizontal direction, the material in the surface layer (above the shear band) is free to move vertically. We observe this experimentally by calculating the velocity field in the region from the fast video data. The shear band in the corners of the system thus acts as an inclined plane and transforms the horizontal motion of the material into vertical motion. Gravity couples to this vertical motion in much the same way it does in the vertical excitation case, which provides the symmetry breaking necessary for driving the period doubling and, at larger Γ, period quadrupling. This response is fed back to the material constrained to horizontal motion via the interaction at the inclined shear band. The fact that the period-doubling field is horizontal below the shear band, and vertical above it [Fig. 13(a)] supports this model. The fact that we observe no hysteresis, and a very weak frequency dependence of Γ', further strengthens the parallel between the proposed model and the vertically excited case [28].

In addition, the localization of the period-doubling response to upper corners of the system explains the differences in measured onset values of Γ: 3.7 at τ_g bifurcation, but as much as 4.5 when observed in the depth profiles of velocity fields. As the period doubling field decays rapidly away from the corners, it takes much higher Γ values for it to become detectable at greater distance. In fact, period-doubling fields calculated very close to the top corners show period doubling already at $\Gamma = 3.5$.

V. CONCLUSIONS

This experiment has studied the responses of a granular system across two orders of magnitude in relevant time scales. We observe and describe the harmonic, subharmonic, and convective response, and also the shearing and the gap opening at the side walls. The specific boundary conditions, which include a shearing surface orthogonal to the direction of gravity, give rise to a surface layer on all time scales.

This surface layer is well defined and maintained across all observed time scales, and it relates the shearing of the material to all other observed responses in the system. The coupling between shear and harmonic response is bidirectional on the one hand, the rubbing of the grains in the shear band leads to energy dissipation and amplitude decay. On the other, the gradients in amplitude and phase of horizontal harmonic motion give rise to shearing in the material. Notably, all of the shear in the system can be accounted for by the harmonic response—there are no faster processes contributing to it. Further, the surprising coincidence of characteristic depths for shearing and harmonic response, and for convection leads to a refinement of the current model for convection in horizontally vibrated systems. Finally, the period doubling was found to be a signature of the internal degrees of freedom, rather than a single-body response. It can be understood through a two-body model in which the shear band acts as an inclined plane in the upper corners of the system, transforming horizontal into vertical motion.

Like the surface layer, the gap is also related to all responses in the system: it is shaped by the harmonic response, it exhibits period doubling and quadrupling, and it drives the convection via avalanching. The depth of the gap corresponds to the total fluidization depth in the system and, in addition, a variety of physical quantities describing the system responses, as well as the convection pattern, do not change with increasing Γ after the gap has reached the full depth of the system.

As the motion of the bulk and the surface layer are decoupled for all responses, there are always internal degrees of freedom excited, which is unlike the case for vertically vibrated systems. In fact, all the observed responses now arise through essentially new mechanisms. This can also be partly ascribed to the restored symmetry of excitation, as, under vertical vibration, gravitational symmetry breaking is responsible for much of the system response.

In conclusion, looking at the responses over a wide range of time scales revealed many important relationships between the observed responses. These results present an additional challenge for the theoretical understanding of granular materials: not only a description of particular responses is needed, but also an explanation of how and why they are interrelated.

ACKNOWLEDGMENTS

The author would like to thank Professor Heinrich M. Jaeger and Professor Sidney R. Nagel, as well as Daniel Mueth for helpful discussions and suggestions. They are also grateful to Professor Michael LaBarbera whose high-speed camera was used in the early setup of the experiment. This research was funded by NSF under Grant No. CTS-9710991 and by the MRSEC program of the NSF under Grant No. DMR-9808595.

[1] H. M. Jaeger, S. R. Nagel, and R. P. Behringer, Rev. Mod. Phys. **68**, 1259 (1996).

[2] P. Evesque, Contemp. Phys. **33**, 245 (1992).

[3] J. A. C. Gallas, H. J. Herrmann, and S. Sokolowski, Phys. Rev. Lett. **69**, 1371 (1992).

[4] J. B. Knight *et al.*, Phys. Rev. E **54**, 5726 (1995).

[5] I. Ippolito, C. Annic, J. Lemaître *et al.*, Phys. Rev. E **52**, 2072 (1995).
[6] S. N. Coppersmith *et al.*, Phys. Rev. E **53**, 4673 (1996).
[7] F. Radjai *et al.*, Phys. Rev. Lett. **77**, 274 (1996).
[8] D. M. Mueth, H. M. Jaeger, and S. R. Nagel, Phys. Rev. E **57**, 3164 (1998).
[9] S. McNamara and S. Luding, Phys. Rev. E **58**, 2247 (1998).
[10] A. Puglisi *et al.*, Phys. Rev. Lett. **81**, 3848 (1998).
[11] J. S. Olafsen and J. S. Urbach, Phys. Rev. Lett. **81**, 4369 (1998).
[12] D. Howell, R. P. Behringer, and C. Veje, Phys. Rev. Lett. **82**, 5241 (1999).
[13] M. Medved, *et al.*, Chaos **9**, 691 (1999).
[14] M. Medved, H. M. Jaeger, and S. R. Nagel, Europhys. Lett. **52**, 66 (2000).
[15] M. Medved, H. M. Jaeger, and S. R. Nagel, Phys. Rev. E **63**, 061302 (2001).
[16] E. R. Nowak *et al.*, Phys. Rev. E **57**, 1971 (1998).
[17] K. L. Gavrilov, Phys. Rev. E **58**, 1 (1998).
[18] A. J. Liu and S. R. Nagel, Nature (London) **396**, 21 (1998).
[19] C. S. O'Hern *et al.*, e-print cond-mat/0005035.
[20] M.-L. Tan and I. Goldhirsch, Phys. Rev. Lett. **81**, 3022 (1998).
[21] P. K. Haff, J. Fluid Mech. **134**, 401 (1983).
[22] J. T. Jenkins and S. B. Savage, J. Fluid Mech. **130**, 187 (1983).
[23] I. Goldhirsch, Chaos **9**, 659 (1999).
[24] L. P. Kadanoff, Rev. Mod. Phys. **71**, 435 (1999).
[25] J. B. Knight, Phys. Rev. E **55**, 6016 (1997).
[26] E. L. Grossman, Phys. Rev. E **56**, 3290 (1997).
[27] K. Liffman, G. Metcalfe, and P. Cleary, Phys. Rev. Lett. **79**, 4574 (1997).
[28] S. G. K. Tennakoon, L. Kondic, and R. P. Behringer, Europhys. Lett. **99**, 1 (1998).
[29] P. Evesque, E. Szmatula, and J.-P. Denis, Europhys. Lett. **12**, 623 (1990).
[30] G. H. Ristow, G. Straßburger, and I. Rehberg, Phys. Rev. Lett. **79**, 833 (1997).
[31] B. Drossel and T. Prellberg, Eur. Phys. J. B **1**, 533 (1998).
[32] A. Kudrolli, M. Wolpert, and J. P. Gollub, Phys. Rev. Lett. **78**, 1383 (1997).
[33] O. Pouliquen, M. Nicolas, and P. D. Weidman, Phys. Rev. Lett. **79**, 3640 (1997).
[34] T. Pöschel and D. E. Rosenkranz, in *A Perspective Look at Nonlinear Media in Physics, Chemistry, and Biology*, edited by J. Parisi, S. C. Müller, and W. Zimmermann (Springer, Berlin, 1997), p. 96.
[35] S. G. K. Tennakoon and R. P. Behringer, Phys. Rev. Lett. **81**, 794 (1998).
[36] M. L. Hunt *et al.*, Phys. Fluids **11**, 68 (1999).
[37] F. Melo, P. Umbanhowar, and H. L. Swinney, Phys. Rev. Lett. **75**, 3838 (1995).
[38] L. S. Tsimring and I. S. Aranson, Phys. Rev. Lett. **79**, 213 (1997).
[39] E. Cerda, F. Melo, and S. Rica, Phys. Rev. Lett. **79**, 4570 (1997).
[40] C. Bizon *et al.*, Phys. Rev. Lett. **80**, 57 (1998).
[41] S. C. Venkataramani and E. Ott, Phys. Rev. Lett. **80**, 3495 (1998).
[42] H. Takahashi, A. Suzuki, and T. Tanaka, Powder Technol. **2**, 65 (1968).
[43] J. M. Luck and A. Mehta, Phys. Rev. E **48**, 3988 (1993).